STRUCTURAL CHEMISTRY

ISSN 2053-2296

Synthesis, structure and orange-light emission of a zero-dimensional antimony(III) halide with the 4,4′-(ethane-1,2-diyl)dipyridin-1-ium cation

Ting Li,[a] Yan-Hong Li,[a] Jia-Yi Han,[a] Yi-Tong Wang[b] and Min-Le Han[a]*

[a]College of Chemistry and Chemical Engineering, Luoyang Normal University, Luoyang 471934, People's Republic of China, and [b]Department of Enviromental Scinece and Engineering, North China Electric Power University (Baoding), Baoding 071003, People's Republic of China. *Correspondence e-mail: minle_han@163.com

Received 3 April 2026
Accepted 2 July 2026

Edited by Z. Song, University of Science and Technology Beijing, People's Republic of China

Keywords: crystal structure; 1,2-bis(pyridin-4-ium)ethane; 4,4′-(ethane-1,2-diyl)dipyridin-1-ium; antimony hydrid halide; orange emission; lead-free halide; IOMH.

CCDC reference: 2543274

Supporting information: this article has supporting information at journals.iucr.org/c

Exploring orange-light-emitting lead-free halides with high photoluminescence quantum yields (PLQYs) is a significant challenge in luminescent materials research. Herein, a zero-dimensional organic–inorganic hybrid halide, namely, 4,4′-(ethane-1,2-diyl)dipyridin-1-ium pentachloridoantimonate(III), $(C_{12}H_{14}N_2)[SbCl_5]$ or $[H_2bpa][SbCl_5]$, where bpa is 1,2-bis(pyridin-4-yl)ethane, was synthesized *via* acid solution evaporation. The compound crystallizes in the triclinic space group $P\overline{1}$. The asymmetric unit consists of an $[SbCl_5]^{2-}$ anion and two half $[H_2bpa]^{2+}$ cations. The $[SbCl_5]^{2-}$ anion and $[H_2bpa]^{2+}$ cations are linked *via* intermolecular hydrogen bonds and π–π interactions to form a three-dimensional supramolecular architecture. Significantly, this halide exhibits highly efficient orange-light emission centred at 600 nm, with a PLQY of 65.57%.

1. Introduction

Recently, zero-dimensional (0D) inorganic–organic metal halides (IOMHs) have shown tremendous potential as luminescent materials due to their diversified structures and tunable photoluminescence (PL) (Han *et al.*, 2021; Haque *et al.*, 2025; Cong *et al.*, 2025; Zhou *et al.*, 2026; Toumi *et al.*, 2025; Zouari *et al.*, 2026; Zhao *et al.*, 2026). Generally, 0D IOMHs are composed of isolated metal halide clusters or units and bulky organic cations with a richer structure database and assembly framework (Shentseva *et al.*, 2024*a*; Shentseva *et al.*, 2024*b*; Shentseva *et al.*, 2025*a*; Shentseva *et al.*, 2025*b*). In contrast to high-dimensional halides, 0D IOMHs always show strong quantum/dielectric confinement and possess much softer lattices, leading to an increased exciton binding energy and allowing for self-trapped exciton (STEs) emission with a wide broadband and large Stokes-shifted properties (Morad *et al.*, 2019; Dastidar *et al.*, 2024; Wang *et al.*, 2024). Up to now, lower-energy green, yellow, orange and red emissions have been readily realized in 0D halides.

Sb^{III}-based metal halides with $5s^2$ lone pairs exhibit the unique advantages of long-wavelength emission in 0D emitters. Great efforts have been devoted to exploring the preparation of 0D lead-free Sb^{III}-based IOMHs (Zhou *et al.*, 2018; Huang *et al.*, 2025; Lv *et al.*, 2025; Lin *et al.*, 2020; Vovna *et al.*, 2015). $[SbX_5]^{2-}$ units typically exhibit efficient broadband emission due to STEs, which is generated by exciton–lattice interactions and structural rearrangement in the excited state (Li *et al.*, 2021). For instance, Ma and co-workers reported an Sb^{III}-based 0D hybrid, $(C_9NH_{20})_2[SbCl_5]$, exhibiting a bright-orange emission and a near-unity photoluminescence quantum yield (PLQY) (98 ± 2%) (Zhou *et al.*, 2018). Du and

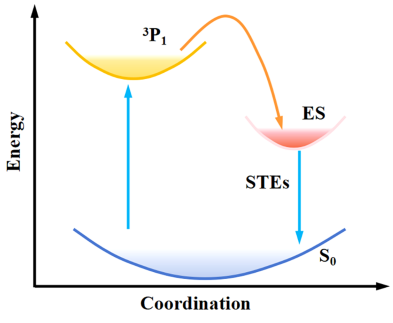

co-workers have reported a series of 0D hybrid Sb^{III}-based 0D hybrids of $ASbCl_5$ (A = $[C_3mmim]^+$, $[C_5mmim]^+$ and $[C_5mim]^+$, where $[C_3mmim]^+$ is 2,3-dimethyl-1-propylimidazolium, $[C_5mmim]^+$ is 2,3-dimethyl-1-pentylimidazolium and $[C_5mim]^+$ is 3-methyl-1-pentylimidazolium) based on discrete $[SbCl_5]^{2-}$ units exhibiting yellow or orange–yellow emission and a maximum PLQY of 79.5% (Chen *et al.*, 2025). It is worth noting that many IOMH systems containing $[SbCl_5]^{2-}$ exhibit high PLQYs (>50%) due to their STEs. This remarkable property has garnered significant attention with respect to efficient solid-state luminescent materials (Jing *et al.*, 2021; Wang *et al.*, 2022).

In the synthetic strategies for organic–inorganic hybrid metal halides, pyridine-based organic molecules, such as bipyridine, are commonly used as cation sources. 4,4′-(Ethane-1,2-diyl)dipyridin-1-ium was also adopted as a cation, and two hybrid bismuth(III) halide crystals have been reported (Adonin *et al.*, 2015*a*; Adonin *et al.*, 2015*b*). However, no hybrid Sb^{III}-based halides have been reported using protonated 1,2-bis(pyridin-4-yl)ethane as the organic cation. In the present study, a new 0D IOMH, $[H_2bpa][SbCl_5]$ (Fig. 1), was prepared using 1,2-bis(pyridin-4-yl)ethane as a cation source. This halide exhibited an intense orange emission centred at 600 nm, mainly arising from the STEs of the $[SbCl]^{2-}$ unit with a PLQY of 65.57%. This work provides an efficient strategy to achieve high-efficiency orange emission.

Table 1
Experimental details.

Crystal data	
Chemical formula	$(C_{12}H_{14}N_2)[SbCl_5]$
M_r	485.25
Crystal system, space group	Triclinic, $P\overline{1}$
Temperature (K)	279
a, b, c (Å)	7.1856 (3), 8.7084 (4), 15.3066 (5)
α, β, γ (°)	90.921 (1), 91.486 (1), 113.638 (2)
V (Å^3)	876.79 (6)
Z	2
Radiation type	Mo $K\alpha$
μ (mm^{-1})	2.33
Crystal size (mm)	0.24 × 0.22 × 0.21
Data collection	
Diffractometer	Bruker APEXII CCD
Absorption correction	Multi-scan (*SADABS*; Bruker, 2016)
T_{min}, T_{max}	0.598, 0.746
No. of measured, independent and observed [$I > 2\sigma(I)$] reflections	42381, 4363, 3975
R_{int}	0.051
(sin $\theta/\lambda)_{max}$ (Å^{-1})	0.667
Refinement	
$R[F^2 > 2\sigma(F^2)]$, $wR(F^2)$, S	0.022, 0.052, 1.08
No. of reflections	4363
No. of parameters	245
No. of restraints	225
H-atom treatment	H-atom parameters constrained
$\Delta\rho_{max}$, $\Delta\rho_{min}$ (e Å^{-3})	0.46, −0.54

Computer programs: *APEX2* (Bruker, 2016), *SAINT* (Bruker, 2016), *olex2.solve* (Bourhis *et al.*, 2015), *SHELXL2014* (Sheldrick, 2015) and *OLEX2* (Dolomanov *et al.*, 2009).

2. Experimental

2.1. Materials and methods

Antimony trichloride (anhydrous, $SbCl_3$, 99.9%) and 1,2-bis(pyridin-4-yl)ethane (bpa, 99.8%) were purchased from Alfa, and hydrogen chloride (HCl, 38%) was purchased from Aladdin. All chemicals are used directly without further purification. Elemental analysis for C, N and H was performed on a Flash2000 organic elemental analyzer. Thermogravimetric analysis was performed on a NETZSCH STA449C microanalyzer heated from 30 to 400 °C in an air atmosphere. Powder X-ray diffraction (PXRD) patterns were taken on a Rigaku D/Max 2500 powder X-ray diffractometer using Cu $K\alpha$ radiation (λ = 1.5418 Å) at a voltage of 40 kV and 40 mA. PL spectra, quantum yield and time-resolved decay spectra were recorded on an Edinburgh FLS1000 fluorescence spectrometer with a xenon lamp and an integrated sphere sample chamber.

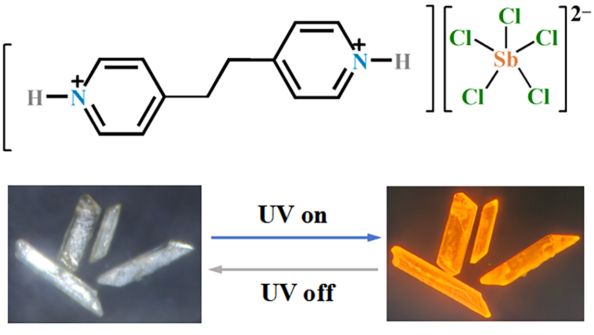

Figure 1
Schematic representation of the structure of $[H_2bpa][SbCl_5]$ (top) and crystal photos of the compound under daylight (left bottom) and 365 nm UV light (right bottom).

2.2. Synthesis of $[H_2bpa][SbCl_5]$

A mixture of bpa (0.01 mmol) and $SbCl_3$ (0.02 mmol) was dissolved in a solution of HCl (1 ml) and stirred at 353 K for 30 min. Light-yellow block-shaped crystals were obtained by slow evaporation under ambient conditions for 1 d. The crystals were collected, washed with acetone five times and then dried in air (yield 63.5%, based on bpa). Analysis calculated (%) for $C_{12}H_{14}Cl_5N_2Sb$: C 29.70, H 2.91, N 5.77; found: C 30.24, H 2.94, N 5.83.

2.3. Refinement

Crystal data, data collection and structure refinement details are summarized in Table 1. H atoms on C and N atoms were located at geometrically calculated positions. The $[H_2bpa]^{2+}$ cation containing atom N2 is entirely disordered. Rings N2/C7–C11 and N2*A*/C7*A*–C11*A* were disordered over two sites with occupancies of 0.649 (10) and 0.351 (10).

2.4. Density functional theory (DFT) calculations

First-principles calculations were carried out using the projected augmented wave (PAW) method (Kresse *et al.*,

1996), as implemented in *VASP* (Kresse *et al.*, 1999; Perdew *et al.*, 1992). The exchange correlation energy was treated using the Perdew–Burke–Ernzerhof (PBE) exchange-correlation functional in the scheme of generalized gradient approximation (Hohenberg *et al.*, 1964; Perdew *et al.*, 1996). The kinetic energy cutoff for all cases was determined to be 520 eV. The convergence thresholds for the electronic calculations and ionic relaxations were chosen as 10^{-6} eV and 0.01 eV Å^{-1}, respectively. The standard Monkhorst–Pack *k*-point grids with a density of 0.1 Å^{-1} were used for Brillouin zone sampling. The valence electron configurations applied in this work were treated as Sb $5s^25p^3$, C $2s^22p^2$, Cl $3s^23p^5$, N $2s^22p^3$ and H $1s^1$. Owing to atomic disorder, each atom is split into two atoms through symmetry operations, corresponding to the presence of two molecules. For theoretical calculations, one set of these molecules is selected for computation (Wu *et al.*, 2026; Ogawa *et al.*, 2020).

3. Results and discussion

Single-crystal X-ray diffraction analysis revealed that $[H_2bpa][SbCl_5]$ crystallizes in the triclinic space group $P\overline{1}$. The asymmetric unit consisted of two half $[H_2bpa]^{2+}$ cations and one $[SbCl_5]^{2-}$ anion. As shown in Fig. 2(*a*), each Sb^{III} ion is coordinated to five Cl^- anions to form a distorted tetragonal $[SbCl_5]^{2-}$ unit, yielding a zero-dimensional (0D) structure. The Sb—Cl bond lengths range from 2.3610 (6) to 2.7621 (6) Å and the Cl—Sb—Cl angles range from 86.30 (3) to 91.58 (2)°, which are comparable to literature values (Peng *et al.*, 2023; Wang *et al.*, 2019). There exist intermolecular hydrogen-bonding interactions between the $[H_2bpa]^{2+}$ cations and the $[SbCl_5]^{2-}$ anions, with N···Cl = 3.0605 (19) and 3.0590 (9) Å, and C···Cl = 3.4540 (2), 3.5300 (2) and 3.5476 (18) Å. Thus, the $[SbCl_5]^{2-}$ tetragonal pyramidal units connect $[H_2bpa]^{2+}$ cations *via* intermolecular hydrogen bonds to form a two-dimensional (2D) layer [Fig. 2(*b*)]. The two pyridinium rings of one $[H_2bpa]^{2+}$ cation are arranged parallel to other $[H_2bpa]^{2+}$ cations in adjacent layers, with interplanar distances of 3.748 and 3.987 Å [Fig. 2(*c*)]. Such 2D layers are further stacked into a three-dimensional (3D) supramolecular architecture. The degree of structural distortion of the $[SbCl_5]^{2-}$ pyramid was evaluated by calculating the angular distortion parameter (σ^2) according to the equation of Robinson *et al.* (1971). The calculated σ^2 value is 2.91 and such a degree of distortion (Li *et al.*, 2019; Peng *et al.*, 2023) suggests the generation of self-trapped excitons (STEs).

The powder X-ray diffraction (PXRD) pattern of $[H_2bpa][SbCl_5]$ matched well with that simulated from the single-crystal structure data, indicating high phase purity [Fig. 3(*a*)]. The thermogravimetric (TG) curve showed that the $[H_2bpa][SbCl_5]$ crystals exhibited excellent thermal stability and begin to decompose from approximately 200 °C [Fig. 3(*b*)].

The photophysical properties of $[H_2bpa][SbCl_5]$ were investigated. As shown in Fig. 4(*a*), the solid-state UV–Vis absorption spectrum of $[H_2bpa][SbCl_5]$ exhibited a band edge at approximately 400 nm [Fig. 4(*a*)]. To characterize the optical properties of $[H_2bpa][SbCl_5]$, the steady-state and time-resolved photoluminescence (PL) spectra were measured. Upon 360 nm excitation, $[H_2bpa][SbCl_5]$ exhibited a bright-orange-emitting band centred at 600 nm, with a full-width at half-maximum (FWHM) of 100 nm and a large Stokes shift of 245 nm [Fig. 4(*b*)]. The Commission Internationale de l'Éclairage (CIE 1931) chromaticity coordinates were determined as (0.52, 0.46) [Fig. 4(*c*)]. The PL decay lifetime was 1.52 ns at 600 nm [Fig. 4(*d*)]. The title compound exhibits a PL quantum yield (PLQY) value of 65.57%, which was moderate among this class of compounds (Zhang *et al.*, 2021; Luo *et al.*, 2022; Peng *et al.*, 2021; Peng *et al.*, 2022; Peng *et al.*, 2023; Li *et al.*, 2019).

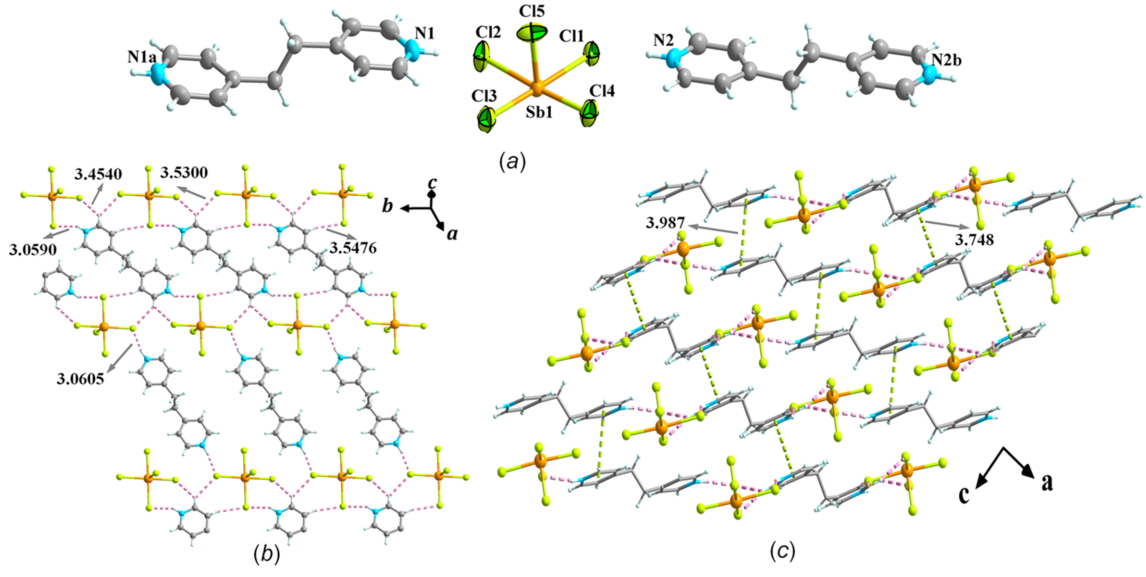

Figure 2
The molecular structure of $[H_2bpa][SbCl_5]$, showing (*a*) the pyramidal $[SbCl_5]^{2-}$ anion and $[H_2bpa]^{2+}$ cation [symmetry codes: (a) $-x+3, -y, -z+1$; (b) $-x+1, -y+1, -z+2$], (*b*) the 2D layer and (*c*) the 3D supramolecular structure.

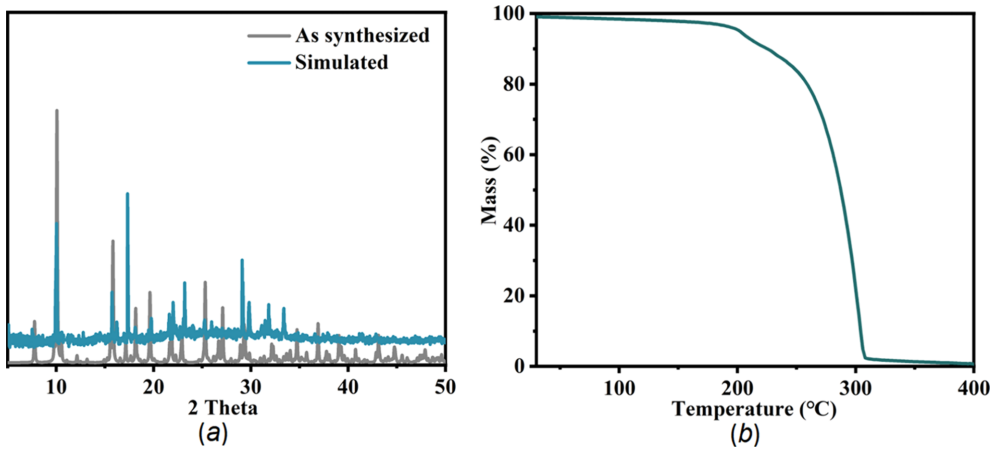

Figure 3
The basic characterization of $[H_2bpa][SbCl_5]$, showing (*a*) the experimental and simulated PXRD patterns of $[H_2bpa][SbCl_5]$, and (*b*) the thermal analysis of $[H_2bpa][SbCl_5]$.

To better understand the luminescence mechanism of $[H_2bpa][SbCl_5]$, density functional theory (DFT) calculations were performed to investigate the band structure and density of states (DOS). The valence band maximum (VBM) of $[H_2bpa][SbCl_5]$ was mainly located on the $[H_2bpa]^{2+}$ cation and Cl atoms, and the conduction band minimum (CBM) was distributed over the $[SbCl_5]^{2-}$ anion [Fig. 4(*e*)]. The energy band gap between the valence and conduction bands of $[H_2bpa][SbCl_5]$ was 2.32 eV [Fig. 4(*f*)], and such a small value indicates a pronounced quantum confinement effect. Meanwhile, these energy band distributions indicated that there was a spatial charge separation between the $[SbCl_5]^{2-}$anion and the $[H_2bpa]^{2+}$ cation, and the charge transfer (CT) may be generated from the $[SbCl_5]^{2-}$anion to the $[H_2bpa]^{2+}$ cation. Considering the weak blue-light emission from the organic ligand, these results further confirmed that the intense orange emission of $[H_2bpa][SbCl_5]$ originated from STEs of the $[SbCl_5]^{2-}$ nodes (Ren *et al.*, 2024; Zhou *et al.*, 2024), and the whole emission contained the contribution of CT from the $[SbCl_5]^{2-}$ anion to the $[H_2bpa]^{2+}$ cation (Qi *et al.*, 2022; An *et*

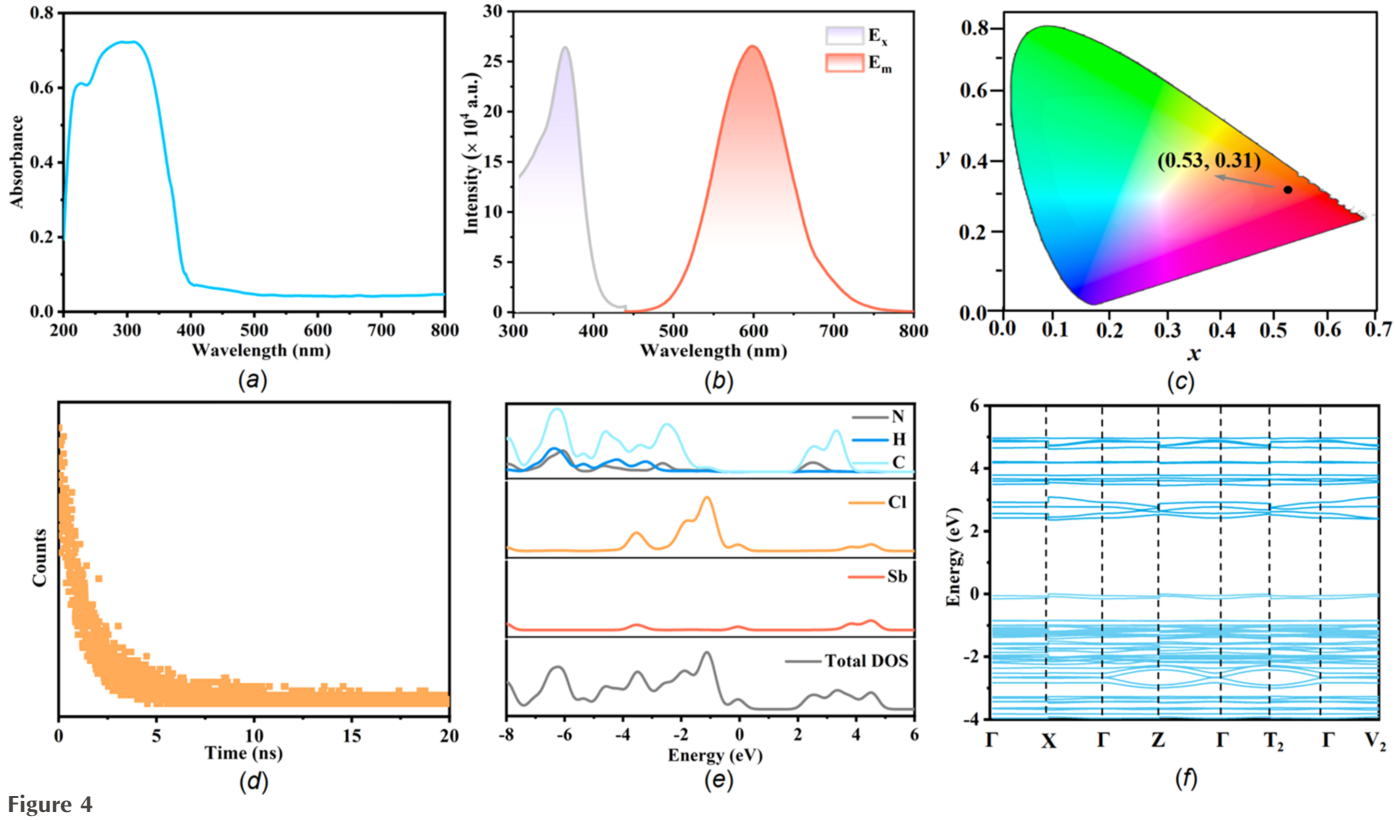

Figure 4
The luminescence properties and theoretical calculations for $[H_2bpa][SbCl_5]$, showing (*a*) the solid-state UV–Vis absorption of $[H_2bpa][SbCl_5]$, (*b*) the excitation and emission spectra of the organic molecule of $[H_2bpa][SbCl_5]$, (*c*) the CIE chromaticity coordinates and (*d*) the PL decay curves of $[H_2bpa][SbCl_5]$. Theoretical calculations for $[H_2bpa][SbCl_5]$, showing (*e*) DOS and (*f*) the calculated band structure.

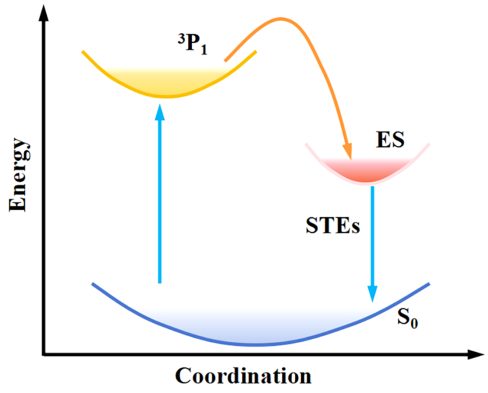

Figure 5
Possible photophysical mechanism for $[H_2bpa][SbCl_5]$.

al., 2024). The photophysical processes can be summarized as follows: Sb^{III} has a typical $5s^2$ electronic configuration, the ground state is $^1S_0$, the excited states of the $5s^15p^1$ configuration contain a singlet state ($^1P_1$) and triplet states (^3P_n, n = 0, 1 and 2) (Jing *et al.*, 2021). As shown in Fig. 5, under excitation at 365 nm, the electrons were excited to the $^3P_1$ state, followed by intersystem crossing to the emitting state (ES), forming triplet excitons. The transition of triplet $^3P_1$ to ground state $^1S_0$ generated the low-energy emission.

4. Summary

Using 1,2-bis(pyridin-4-yl)ethane, an antimony-based hybrid halide has been prepared. It exhibited efficient orange emission with a high PLQY of 65.57%. Experimental and theoretical studies indicated that the emission originated from the synergistic contribution of electron transitions in the organic cations and STE states. This work lays the foundation for synthesizing more-efficient orange-emitting hybrid halides.

Conflict of interest

The authors declare that there are no conflicts of interests.

Funding information

Funding for this research was provided by: Program for Innovative Research Team from the University of Henan Province (grant No. 24IRTSTHN005).

References

Adonin, S. A., Rakhmanova, M. E., Samsonenko, D. G., Sokolov, M. N. & Fedin, V. P. (2015*a*). *Polyhedron* **98**, 1–4.
Adonin, S. A., Rakhmanova, M. E., Smolentsev, A. I., Korolkov, I. V., Sokolov, M. N. & Fedin, V. P. (2015*b*). *New J. Chem.* **39**, 5529–5533.
An, S., Qiao, M., Jin, X., Chen, X., Su, J., Guo, L. & Zhang, Z. (2024). *Sci. China Chem.* **67**, 512–516.
Bourhis, L. J., Dolomanov, O. V., Gildea, R. J., Howard, J. A. K. & Puschmann, H. (2015). *Acta Cryst.* A**71**, 59–75.
Bruker (2016). *APEX2*, *SAINT* and *SADABS*. Bruker AXS Inc., Madison, Wisconsin, USA.
Chen, G., Guo, X., Lin, H., Zhang, Z., Ablez, A., Ren, Y., Du, K. & Huang, X. (2025). *Molecules* **30**, 3431.
Cong, L., Jia, Y., Cheng, X., Liu, Y., Li, J. & Cui, B.-B. (2025). *Adv. Opt. Mater.* **13**, e00902.
Dastidar, R. G., Okamoto, T., Takahashi, K., Takano, Y., Vijayakumar, C., Subrahmanyam, C. & Biju, V. (2024). *Nanoscale* **16**, 5107–5114.
Dolomanov, O. V., Bourhis, L. J., Gildea, R. J., Howard, J. A. K. & Puschmann, H. (2009). *J. Appl. Cryst.* **42**, 339–341.
Han, Y., Yue, S. & Cui, B. B. (2021). *Adv. Sci.* **8**, 2004805.
Haque, M. A., Grieder, A., Harvey, S. P., Brunecky, R., Ye, J. Y., Addison, B., Zhang, J., Dong, Y., Xie, Y., Hautzinger, M. P., Walpitage, H. H., Zhu, K., Blackburn, J. L., Vardeny, Z. V., Mitzi, D. B., Berry, J. J., Marder, S. R., Ping, Y., Beard, M. C. & Luther, J. M. (2025). *Nat. Chem.* **17**, 29–37.
Hohenberg, P. & Kohn, W. (1964). *Phys. Rev.* **136**, B864–B871.
Huang, T., Peng, H., Zeng, R. & Zou, B. (2025). *Adv. Funct. Mater.* **35**, e11803.
Jing, Y., Liu, Y., Li, M. & Xia, Z. (2021). *Adv. Opt. Mater.* **9**, 2002213.
Kresse, G. & Furthmüller, J. (1996). *Phys. Rev. B* **54**, 11169–11186.
Kresse, G. & Joubert, D. (1999). *Phys. Rev. B* **59**, 1758–1775.
Li, M. & Xia, Z. (2021). *Chem. Soc. Rev.* **50**, 2626–2662.
Li, Z., Li, Y., Liang, P., Zhou, T., Wang, L. & Xie, R.-J. (2019). *Chem. Mater.* **31**, 9363–9371.
Lin, F., Wang, H., Liu, W. & Li, J. (2020). *J. Mater. Chem. C* **8**, 7300–7303.
Luo, J.-B., Wei, J.-H., Zhang, Z.-Z. & Kuang, D.-B. (2022). *Inorg. Chem.* **61**, 338–345.
Lv, W., Liu, P., Yu, Y., Cai, Y., Wei, W., Han, C., Miao, Z., Xu, L., Wu, G., Liu, Z. & Chen, R. (2025). *Inorg. Chem.* **64**, 19404–19412.
Morad, V., Shynkarenko, Y., Yakunin, S., Brumberg, A., Schaller, R. D. & Kovalenko, M. V. (2019). *J. Am. Chem. Soc.* **141**, 9764–9768.
Ogawa, N., Nagase, H., Matsumoto, T., Kaga, M., Ishihara, S., Endo, T., Yasunaga, T., Kawashima, Y., Ueda, H. & Yamamoto, H. (2020). *Int. J. Pharm.* **587**, 119625.
Peng, Y.-C., Jin, J.-C., Gu, Q., Dong, Y., Zhang, Z.-Z., Zhuang, T.-H., Gong, L.-K., Ma, W., Wang, Z.-P., Du, K.-Z. & Huang, X.-Y. (2021). *Inorg. Chem.* **60**, 17837–17845.
Peng, Y.-C., Lin, H.-W., Zhou, S.-H., Jin, J.-C., Zhuang, T.-H., Ablez, A., Wang, Z.-P., Du, K.-Z. & Huang, X.-Y. (2023). *Molecules* **28**, 1978.
Peng, Y.-C., Zhou, S.-H., Jin, J.-C., Zhuang, T.-H., Gong, L.-K., Lin, H.-W., Wang, Z.-P., Du, K.-Z. & Huang, X.-Y. (2022). *J. Phys. Chem. C* **126**, 17381–17389.
Perdew, J. P., Burke, K. & Ernzerhof, M. (1996). *Phys. Rev. Lett.* **77**, 3865–3868.
Perdew, J. P., Chevary, J. A., Vosko, S. H., Jackson, K. A., Pederson, M. R., Singh, D. J. & Fiolhais, C. (1992). *Phys. Rev. B* **46**, 6671–6687.
Qi, Z., Gao, H., Zhu, X., Lu, Z. & Zhang, X. (2022). *Inorg. Chem.* **61**, 19483–19491.
Ren, Q., Zhou, G., Mao, Y., Zhang, J., Zhang, J. & Zhang, X. M. (2024). *Chem. Sci.* **15**, 16536–16545.
Robinson, K., Gibbs, G. V. & Ribbe, P. H. (1971). *Science* **172**, 567–570.
Sheldrick, G. M. (2015). *Acta Cryst.* C**71**, 3–8.
Shentseva, I. A., Tagiltsev, K. A., Usol'tsev, A. N., Korobeynikov, N. A., Shayapov, V. R., Sokolov, M. N. & Adonin, S. A. (2024*b*). *Russ. J. Inorg. Chem.* **69**, 1158–1164.
Shentseva, I. A., Usol'tsev, A. N., Korobeinikov, N. A. & Adonin, S. A. (2024*a*). *Russ. J. Coord. Chem.* **50**, 809–816.
Shentseva, I. A., Usol'tsev, A. N., Korobeinikov, N. A., Sokolov, M. N. & Adonin, S. A. (2025*a*). *Russ. J. Coord. Chem.* **51**, 795–805.
Shentseva, I. A., Usoltsev, A. N., Korobeynikov, N. A., Sokolov, M. N. & Adonin, S. A. (2025*b*). *J. Struct. Chem.* **66**, 2090–2095.
Toumi, E., Elleuch, N., Shova, S. & Boujelbene, M. (2025). *J. Mol. Struct.* **1347**, 143291.

Vovna, V. I., Dotsenko, A. A., Korochentsev, V. V., Shcheka, O. L., Os'mushko, I. S., Mirochnik, A. G., Sedakova, T. V. & Sergienko, V. I. (2015). *J. Mol. Struct.* **1091**, 138–146.
Wang, Y., Liu, J., Liu, Y., Li, S., Xu, X. & Lou, Z. (2024). *J. Mater. Chem. C* **12**, 10267–10329.
Wang, Z. & Huang, X. (2022). *Chem. A Eur. J.* **28**, e202200609.
Wang, Z., Zhang, Z., Tao, L., Shen, N., Hu, B., Gong, L., Li, J., Chen, X. & Huang, X. (2019). *Angew. Chem. Int. Ed.* **58**, 9974–9978.
Wu, L., Jiang, C., Xing, R., Bai, J., Li, J. & Xie, Z. (2026). *J. Mol. Struct.* **1376**, 147029.
Zhang, Z., Lin, Y., Jin, J., Gong, L., Peng, Y., Song, Y., Shen, N., Wang, Z., Du, K. & Huang, X. (2021). *Angew. Chem. Int. Ed.* **60**, 23373–23379.
Zhao, Y.-Y., Chen, J.-C., Zhang, L., Chen, J., Liao, Q., Li, Z.-Q., Lin, M., Yao, J. & Zhong, Y.-W. (2026). *Chem. Sci.* **17**, 2340–2347.
Zhou, C. K., Lin, H. R., Tian, Y., Yuan, Z., Clark, R., Chen, B. H., van de Burgt, L. J., Wang, J. C., Zhou, Y., Hanson, K., Meisner, Q. J., Neu, J., Besara, T., Siegrist, T., Lambers, E., Djurovich, P. & Ma, B. W. (2018). *Chem. Sci.* **9**, 586–593.
Zhou, G., Wang, S., Zhang, N., Mao, Y., Zhou, J., Xia, Z. & Zhang, X.-M. (2026). *Adv. Funct. Mater.* **36**, e20933.
Zhou, G., Wang, Y., Mao, Y., Guo, C., Zhang, J., Molokeev, M. S., Xia, Z. & Zhang, X.-M. (2024). *Adv. Funct. Mater.* **34**, 2401860.
Zouari, C., Alibi, A., Shova, S., Boujelbene, M. & Abdelhedi, M. (2026). *J. Mol. Struct.* **1352**, 144507.

supporting information

Acta Cryst. (2026). C**82**, 453-458 [https://doi.org/10.1107/S2053229626006935]

Synthesis, structure and orange-light emission of a zero-dimensional antimony(III) halide with the 4,4′-(ethane-1,2-diyl)dipyridin-1-ium cation

Ting Li, Yan-Hong Li, Jia-Yi Han, Yi-Tong Wang and Min-Le Han

Computing details

4,4′-(Ethane-1,2-diyl)dipyridin-1-ium pentachloridoantimonate(III)

Crystal data

$(C_{12}H_{14}N_2)[SbCl_5]$
$M_r = 485.25$
Triclinic, $P\overline{1}$
$a = 7.1856$ (3) Å
$b = 8.7084$ (4) Å
$c = 15.3066$ (5) Å
$\alpha = 90.921$ (1)°
$\beta = 91.486$ (1)°
$\gamma = 113.638$ (2)°
$V = 876.79$ (6) Å^3
$Z = 2$
$F(000) = 472$
$D_x = 1.838$ Mg m^{-3}
Mo $K\alpha$ radiation, $\lambda = 0.71073$ Å
Cell parameters from 9994 reflections
$\theta = 2.6$–28.2°
$\mu = 2.33$ mm^{-1}
$T = 279$ K
Block, clear light yellow
0.24 × 0.22 × 0.21 mm

Data collection

Bruker APEXII CCD diffractometer
phi and ω scans
Absorption correction: multi-scan (SADABS; Bruker, 2016)
$T_{min} = 0.598$, $T_{max} = 0.746$
42381 measured reflections
4363 independent reflections
3975 reflections with $I > 2\sigma(I)$
$R_{int} = 0.051$
$\theta_{max} = 28.3°$, $\theta_{min} = 2.6°$
$h = -9 \rightarrow 9$
$k = -11 \rightarrow 11$
$l = -20 \rightarrow 20$

Refinement

Refinement on F^2
Least-squares matrix: full
$R[F^2 > 2\sigma(F^2)] = 0.022$
$wR(F^2) = 0.052$
$S = 1.08$
4363 reflections
245 parameters
225 restraints
Primary atom site location: iterative
Hydrogen site location: inferred from neighbouring sites
H-atom parameters constrained
$w = 1/[\sigma^2(F_o^2) + (0.0217P)^2 + 0.2665P]$ where $P = (F_o^2 + 2F_c^2)/3$
$(\Delta/\sigma)_{max} = 0.001$
$\Delta\rho_{max} = 0.46$ e Å^{-3}
$\Delta\rho_{min} = -0.54$ e Å^{-3}

Special details

Geometry. All esds (except the esd in the dihedral angle between two l.s. planes) are estimated using the full covariance matrix. The cell esds are taken into account individually in the estimation of esds in distances, angles and torsion angles; correlations between esds in cell parameters are only used when they are defined by crystal symmetry. An approximate (isotropic) treatment of cell esds is used for estimating esds involving l.s. planes.

Fractional atomic coordinates and isotropic or equivalent isotropic displacement parameters (Å²)

	x	*y*	*z*	U_{iso}*/U_{eq}	Occ. (<1)
Sb1	1.39542 (2)	0.57078 (2)	0.78279 (2)	0.03821 (5)	
Cl1	1.29721 (9)	0.83104 (7)	0.74427 (4)	0.05346 (13)	
Cl2	1.64670 (11)	0.64297 (7)	0.64208 (5)	0.06858 (18)	
Cl3	1.48129 (13)	0.32296 (9)	0.81640 (4)	0.0742 (2)	
Cl4	1.15174 (11)	0.50357 (9)	0.90359 (4)	0.06879 (18)	
Cl5	1.13542 (11)	0.39669 (8)	0.68422 (4)	0.07420 (19)	
N1	0.6529 (3)	0.3044 (2)	0.58980 (13)	0.0490 (4)	
H1	0.6070	0.3717	0.6137	0.059*	
C1	0.7489 (3)	0.3467 (3)	0.51526 (15)	0.0522 (5)	
H1A	0.7631	0.4463	0.4891	0.063*	
C2	0.8267 (3)	0.2439 (3)	0.47714 (14)	0.0485 (5)	
H2	0.8947	0.2737	0.4251	0.058*	
C3	0.8048 (3)	0.0952 (2)	0.51572 (12)	0.0383 (4)	
C4	0.6984 (3)	0.0543 (2)	0.59228 (14)	0.0448 (4)	
H4	0.6771	−0.0465	0.6188	0.054*	
C5	0.6251 (3)	0.1623 (3)	0.62874 (15)	0.0494 (5)	
H5	0.5559	0.1362	0.6806	0.059*	
C6	0.8967 (3)	−0.0167 (3)	0.47738 (14)	0.0464 (5)	
H6A	0.9145	0.0029	0.4154	0.056*	
H6B	0.8055	−0.1330	0.4842	0.056*	
N2	0.9563 (12)	−0.1343 (9)	0.8473 (5)	0.0493 (15)	0.649 (10)
H2A	1.0322	−0.1649	0.8150	0.059*	0.649 (10)
C7	0.8644 (14)	−0.2304 (9)	0.9129 (6)	0.0480 (14)	0.649 (10)
H7	0.8836	−0.3278	0.9240	0.058*	0.649 (10)
C8	0.741 (2)	−0.1843 (13)	0.9638 (7)	0.0518 (12)	0.649 (10)
H8	0.6683	−0.2549	1.0070	0.062*	0.649 (10)
C9	0.7248 (9)	−0.0318 (7)	0.9514 (4)	0.0473 (12)	0.649 (10)
C10	0.8204 (12)	0.0601 (8)	0.8805 (5)	0.0571 (13)	0.649 (10)
H10	0.8053	0.1586	0.8678	0.068*	0.649 (10)
C11	0.9359 (14)	0.0071 (10)	0.8296 (5)	0.0565 (14)	0.649 (10)
H11	1.0008	0.0697	0.7823	0.068*	0.649 (10)
C12	0.6107 (6)	0.0357 (6)	1.0123 (4)	0.0592 (13)	0.649 (10)
H12A	0.6295	0.0070	1.0719	0.071*	0.649 (10)
H12B	0.6651	0.1570	1.0096	0.071*	0.649 (10)
N2A	0.945 (2)	−0.1733 (17)	0.8602 (10)	0.0462 (19)	0.351 (10)
H2AA	1.0192	−0.2191	0.8372	0.055*	0.351 (10)
C7A	0.833 (3)	−0.2468 (17)	0.9269 (11)	0.047 (2)	0.351 (10)
H7A	0.8296	−0.3485	0.9465	0.057*	0.351 (10)
C8A	0.723 (4)	−0.171 (2)	0.9666 (13)	0.050 (2)	0.351 (10)

H8A	0.6581	−0.2132	1.0181	0.060*	0.351 (10)
C9A	0.7070 (19)	−0.0309 (14)	0.9299 (7)	0.0499 (18)	0.351 (10)
C10A	0.829 (2)	0.0403 (15)	0.8605 (8)	0.054 (2)	0.351 (10)
H10A	0.8285	0.1377	0.8366	0.065*	0.351 (10)
C11A	0.949 (2)	−0.0318 (18)	0.8273 (9)	0.052 (2)	0.351 (10)
H11A	1.0334	0.0176	0.7816	0.063*	0.351 (10)
C12A	0.5700 (14)	0.0473 (10)	0.9664 (7)	0.0543 (19)	0.351 (10)
H12C	0.6552	0.1573	0.9911	0.065*	0.351 (10)
H12D	0.4901	0.0636	0.9183	0.065*	0.351 (10)

Atomic displacement parameters (Å²)

	U^{11}	U^{22}	U^{33}	U^{12}	U^{13}	U^{23}
Sb1	0.04012 (8)	0.03886 (8)	0.03816 (7)	0.01848 (6)	0.00464 (5)	−0.00403 (5)
Cl1	0.0617 (3)	0.0518 (3)	0.0575 (3)	0.0321 (3)	0.0256 (2)	0.0108 (2)
Cl2	0.0908 (4)	0.0482 (3)	0.0842 (4)	0.0428 (3)	0.0490 (4)	0.0208 (3)
Cl3	0.1086 (5)	0.0783 (4)	0.0674 (4)	0.0685 (4)	0.0299 (4)	0.0207 (3)
Cl4	0.0872 (4)	0.0695 (4)	0.0626 (3)	0.0423 (3)	0.0384 (3)	0.0168 (3)
Cl5	0.0758 (4)	0.0600 (4)	0.0627 (4)	0.0036 (3)	−0.0198 (3)	−0.0053 (3)
N1	0.0442 (9)	0.0410 (9)	0.0683 (11)	0.0239 (8)	0.0073 (8)	−0.0053 (8)
C1	0.0533 (12)	0.0447 (11)	0.0626 (13)	0.0234 (10)	0.0004 (10)	0.0099 (10)
C2	0.0512 (12)	0.0526 (12)	0.0427 (10)	0.0215 (10)	0.0055 (9)	0.0063 (9)
C3	0.0347 (9)	0.0381 (9)	0.0422 (9)	0.0150 (8)	0.0007 (7)	−0.0057 (7)
C4	0.0478 (11)	0.0345 (10)	0.0536 (11)	0.0174 (8)	0.0128 (9)	0.0044 (8)
C5	0.0484 (11)	0.0425 (11)	0.0568 (12)	0.0169 (9)	0.0189 (9)	0.0011 (9)
C6	0.0446 (11)	0.0493 (11)	0.0487 (11)	0.0229 (9)	0.0003 (8)	−0.0129 (9)
N2	0.0423 (17)	0.067 (4)	0.043 (2)	0.026 (2)	0.0142 (15)	−0.004 (2)
C7	0.047 (3)	0.060 (2)	0.047 (3)	0.033 (2)	0.011 (2)	0.001 (2)
C8	0.055 (3)	0.063 (2)	0.049 (2)	0.0337 (18)	0.0133 (19)	0.010 (2)
C9	0.0417 (18)	0.059 (2)	0.047 (2)	0.0259 (15)	0.0054 (18)	−0.0053 (17)
C10	0.062 (2)	0.057 (2)	0.060 (3)	0.0318 (18)	0.012 (2)	0.000 (2)
C11	0.056 (2)	0.062 (3)	0.055 (2)	0.025 (2)	0.0167 (18)	0.009 (2)
C12	0.050 (2)	0.073 (2)	0.058 (3)	0.0304 (18)	−0.0026 (18)	−0.018 (2)
N2A	0.047 (3)	0.055 (4)	0.048 (4)	0.033 (3)	0.009 (3)	−0.001 (3)
C7A	0.044 (4)	0.065 (4)	0.038 (4)	0.027 (3)	0.016 (3)	0.009 (3)
C8A	0.050 (4)	0.064 (4)	0.043 (3)	0.030 (3)	0.021 (3)	−0.004 (3)
C9A	0.055 (3)	0.061 (3)	0.047 (4)	0.037 (2)	0.009 (3)	0.001 (3)
C10A	0.066 (4)	0.055 (4)	0.048 (4)	0.030 (3)	0.014 (3)	0.003 (3)
C11A	0.056 (3)	0.056 (4)	0.052 (3)	0.030 (3)	0.018 (3)	0.002 (4)
C12A	0.062 (4)	0.065 (3)	0.050 (4)	0.039 (3)	0.014 (3)	0.014 (3)

Geometric parameters (Å, º)

Sb1—Cl1	2.6993 (5)	C8—H8	0.9300
Sb1—Cl2	2.7621 (6)	C8—C9	1.396 (6)
Sb1—Cl3	2.5278 (6)	C9—C10	1.383 (5)
Sb1—Cl4	2.4916 (6)	C9—C12	1.515 (5)
Sb1—Cl5	2.3610 (6)	C10—H10	0.9300

N1—H1	0.8600	C10—C11	1.356 (6)
N1—C1	1.328 (3)	C11—H11	0.9300
N1—C5	1.326 (3)	C12—C12^{ii}	1.493 (9)
C1—H1A	0.9300	C12—H12A	0.9700
C1—C2	1.362 (3)	C12—H12B	0.9700
C2—H2	0.9300	N2A—H2AA	0.8600
C2—C3	1.384 (3)	N2A—C7A	1.323 (7)
C3—C4	1.388 (3)	N2A—C11A	1.330 (7)
C3—C6	1.499 (3)	C7A—H7A	0.9300
C4—H4	0.9300	C7A—C8A	1.364 (7)
C4—C5	1.367 (3)	C8A—H8A	0.9300
C5—H5	0.9300	C8A—C9A	1.397 (7)
C6—C6^{i}	1.537 (4)	C9A—C10A	1.384 (7)
C6—H6A	0.9700	C9A—C12A	1.516 (6)
C6—H6B	0.9700	C10A—H10A	0.9300
N2—H2A	0.8600	C10A—C11A	1.358 (8)
N2—C7	1.327 (5)	C11A—H11A	0.9300
N2—C11	1.328 (5)	C12A—C12A^{ii}	1.470 (14)
C7—H7	0.9300	C12A—H12C	0.9700
C7—C8	1.363 (5)	C12A—H12D	0.9700

Cl1—Sb1—Cl2	89.768 (16)	C7—C8—C9	120.4 (4)
Cl3—Sb1—Cl1	178.71 (2)	C9—C8—H8	119.8
Cl3—Sb1—Cl2	90.107 (19)	C8—C9—C12	122.9 (4)
Cl4—Sb1—Cl1	88.479 (19)	C10—C9—C8	117.2 (4)
Cl4—Sb1—Cl2	176.62 (2)	C10—C9—C12	119.9 (4)
Cl4—Sb1—Cl3	91.58 (2)	C9—C10—H10	119.9
Cl5—Sb1—Cl1	89.77 (2)	C11—C10—C9	120.3 (4)
Cl5—Sb1—Cl2	86.30 (3)	C11—C10—H10	119.9
Cl5—Sb1—Cl3	88.94 (3)	N2—C11—C10	120.0 (4)
Cl5—Sb1—Cl4	90.80 (3)	N2—C11—H11	120.0
C1—N1—H1	118.8	C10—C11—H11	120.0
C5—N1—H1	118.8	C9—C12—H12A	109.5
C5—N1—C1	122.41 (18)	C9—C12—H12B	109.5
N1—C1—H1A	120.1	C12^{ii}—C12—C9	110.7 (5)
N1—C1—C2	119.88 (19)	C12^{ii}—C12—H12A	109.5
C2—C1—H1A	120.1	C12^{ii}—C12—H12B	109.5
C1—C2—H2	120.0	H12A—C12—H12B	108.1
C1—C2—C3	120.1 (2)	C7A—N2A—H2AA	118.5
C3—C2—H2	120.0	C7A—N2A—C11A	122.9 (6)
C2—C3—C4	117.90 (18)	C11A—N2A—H2AA	118.5
C2—C3—C6	121.25 (18)	N2A—C7A—H7A	120.5
C4—C3—C6	120.83 (18)	N2A—C7A—C8A	119.0 (6)
C3—C4—H4	120.0	C8A—C7A—H7A	120.5
C5—C4—C3	119.95 (19)	C7A—C8A—H8A	119.9
C5—C4—H4	120.0	C7A—C8A—C9A	120.2 (6)
N1—C5—C4	119.74 (19)	C9A—C8A—H8A	119.9
N1—C5—H5	120.1	C8A—C9A—C12A	122.2 (6)

C4—C5—H5	120.1	C10A—C9A—C8A	117.4 (5)
C3—C6—C6^{i}	110.8 (2)	C10A—C9A—C12A	120.4 (6)
C3—C6—H6A	109.5	C9A—C10A—H10A	120.0
C3—C6—H6B	109.5	C11A—C10A—C9A	120.1 (6)
C6^{i}—C6—H6A	109.5	C11A—C10A—H10A	120.0
C6^{i}—C6—H6B	109.5	N2A—C11A—C10A	119.8 (6)
H6A—C6—H6B	108.1	N2A—C11A—H11A	120.1
C7—N2—H2A	118.6	C10A—C11A—H11A	120.1
C7—N2—C11	122.7 (4)	C9A—C12A—H12C	108.2
C11—N2—H2A	118.6	C9A—C12A—H12D	108.2
N2—C7—H7	120.5	C12A^{ii}—C12A—C9A	116.3 (7)
N2—C7—C8	119.1 (4)	C12A^{ii}—C12A—H12C	108.2
C8—C7—H7	120.5	C12A^{ii}—C12A—H12D	108.2
C7—C8—H8	119.8	H12C—C12A—H12D	107.4

N1—C1—C2—C3	0.4 (3)	C8—C9—C12—C12^{ii}	−84.8 (11)
C1—N1—C5—C4	0.6 (3)	C9—C10—C11—N2	0.6 (12)
C1—C2—C3—C4	1.4 (3)	C10—C9—C12—C12^{ii}	96.1 (8)
C1—C2—C3—C6	−177.3 (2)	C11—N2—C7—C8	0.9 (15)
C2—C3—C4—C5	−2.1 (3)	C12—C9—C10—C11	174.9 (7)
C2—C3—C6—C6^{i}	96.3 (3)	N2A—C7A—C8A—C9A	9 (3)
C3—C4—C5—N1	1.2 (3)	C7A—N2A—C11A—C10A	−2 (3)
C4—C3—C6—C6^{i}	−82.3 (3)	C7A—C8A—C9A—C10A	−9 (3)
C5—N1—C1—C2	−1.4 (3)	C7A—C8A—C9A—C12A	173.9 (18)
C6—C3—C4—C5	176.5 (2)	C8A—C9A—C10A—C11A	4 (2)
N2—C7—C8—C9	−4.9 (18)	C8A—C9A—C12A—C12A^{ii}	−9 (2)
C7—N2—C11—C10	1.3 (13)	C9A—C10A—C11A—N2A	2 (2)
C7—C8—C9—C10	6.5 (17)	C10A—C9A—C12A—C12A^{ii}	173.5 (15)
C7—C8—C9—C12	−172.6 (9)	C11A—N2A—C7A—C8A	−3 (3)
C8—C9—C10—C11	−4.3 (12)	C12A—C9A—C10A—C11A	−179.0 (14)

Symmetry codes: (i) −*x*+2, −*y*, −*z*+1; (ii) −*x*+1, −*y*, −*z*+2.